A Cluster of Compact Radio Sources in NGC 2024 (Orion B)

Luis F. Rodríguez and Yolanda Gómez

Centro de Radioastronomía y Astrofísica, UNAM, Apdo. Postal 3-72 (Xangari), 58089 Morelia, Michoacán, México

l.rodriguez, y.gomez@astrosmo.unam.mx

and

Bo Reipurth

Institute for Astronomy, University of Hawaii, 2680 Woodlawn Drive, Honolulu, HI 96822

reipurth@ifa.hawaii.edu

ABSTRACT

We present deep 3.6 cm radio continuum observations of the H II region NGC 2024 in Orion B obtained using the Very Large Array in its A-configuration, with $0\farcs2$ angular resolution. We detect a total of 25 compact radio sources in a region of $4' \times 4'$. We discuss the nature of these sources and its relation with the infrared and X-ray objects in the region. At least two of the radio sources are obscured proplyds whose morphology can be used to restrict the location of the main ionizing source of the region. This cluster of radio sources is compared with others that have been found in regions of recent star formation.

Subject headings: stars: formation – stars: pre-main sequence – ISM: individual (NGC 2024) – binaries: general – radio continuum

1. INTRODUCTION

NGC 2024 is a prominent H II region located in the Orion B (L 1630) star-forming complex, at a distance of ∼415 pc (Anthony-Twarog 1982). The H II region is sharply ionization-bounded to the south (Barnes et al. 1989). With a total flux density of ∼60 Jy at cm wavelengths (Rodríguez & Chaisson 1978; Barnes et al. 1989), the H II region requires about 10^{48} ionizing photons per second to maintain its ionization, a flux that can be provided by an O9 ZAMS star with a luminosity of $\sim 5.0 \times 10^4\ L_\odot$. Until recently, the

required exciting star had not been identified, but Bik et al. (2003) have proposed that the infrared source IRS2b is an embedded late O or early B star responsible for the ionization.

A prominent dust lane is seen in optical images to run across the region from north to south. This dust lane is evident also in molecular line observations of the region (i. e. Schulz et al. 1991). Mezger et al. (1988) identified 6 small-scale submm condensations embedded along this dense ridge, suggesting that star formation is presently taking place here.

Clusters of near-infrared (Lada et al. 1991; Beck et al. 2003; Haisch et al. 2000), mid-infrared (Haisch et al. 2001), and X-ray sources (Skinner, Belzer, & Gagner 2003) are known to exist in association with NGC 2024. Furthermore, a number of submillimeter continuum sources were found and studied by Mezger et al. (1988) and Visser et al. (1998). To provide a more complete census of the young stellar population in this region, we have undertaken deep, high angular resolution 3.6 cm observations in an attempt to detect a cluster of compact radio sources similar to those found in Orion A (Garay, Moran, & Reid 1987; Churchwell et al. 1987), NGC 1333 (Rodríguez, Anglada, & Curiel 1999), the Arches region near the galactic center (Lang, Goss, & Rodríguez 2001), and in GGD 14 (Gómez, Rodríguez, & Garay 2000; 2002).

2. OBSERVATIONS

We have used the Very Large Array of the NRAO[1] in its A-array configuration to observe NGC 2024 at 3.6 cm. The region was observed on 2002 March 2, 3, and 8. Our phase center was at $\alpha(J2000) = 05^h41^m44\overset{s}{.}9$; $\delta(J2000) = -01°55'54''$. The amplitude calibrator was 1331+305, with an adopted flux density of 5.18 Jy, and the phase calibrator was 0541−056, with an average flux density of 0.748±0.004 Jy over the three epochs of observation. The data were analyzed in the standard manner using the package AIPS of NRAO. The data were self-calibrated in phase. Individual images were made at each epoch to search for fast variability (on a timescale of days) between the epochs observed. To diminish the presence of extended emission, in particular that originating from the very sharp ionization front of the H II region that is evident in Fig. 1b of Barnes et al. (1989), we used only visibilities with baselines larger than 100 kλ, thus suppressing the emission of structures larger than $\sim 2''$. The images were restored with a circular beam of $0\overset{''}{.}24$, the average value of the angular resolution of the individual maps made with the ROBUST parameter of IMAGR set to 0. The three maps were then averaged to obtain an rms noise of 15 μJy.

[1]The National Radio Astronomy Observatory is a facility of the National Science Foundation operated under cooperative agreement by Associated Universities, Inc.

A total of 25 sources were detected in a region of $4' \times 4'$. The distribution of these sources is shown in Figure 1. Following Fomalont et al. (2002), we estimate that in a field of $4' \times 4'$ the *a priori* number of expected 3.6 cm sources above 0.1 mJy is $\sim$0.6. We then conclude that probably one out of the 25 sources could be a background object, but that we are justified in assuming that practically all the members of the radio cluster are associated with NGC 2024. In Figure 2 we show the positions of the radio sources overlapped on the red DSS2 image of the region. From this figure it is evident that the cluster of radio sources is closely associated with the central parts of the dust lane that runs across NGC 2024.

In Table 1 we list the positions and flux densities of the sources, averaged over the three observations. We also note in column 5 if they were found to be variable or not. The number given in parenthesis for the variable sources is the ratio between the largest and smallest flux density observed. Finally, in the last three columns we list counterparts, when found. A counterpart was taken as such if its position was within $3''$ of the radio position. The radio positions are estimated to be accurate to $\sim 0\farcs05$.

3. OVERALL CHARACTERISTICS OF THE SAMPLE OF RADIO SOURCES

Out of the 25 radio sources detected, 13 have a 2MASS counterpart and 15 have a Chandra counterpart (Skinner et al. 2003). Only the brightest source in the radio cluster, VLA 19, had been previously reported at radio wavelengths (Snell & Bally 1986; Gaume, Johnston, & Wilson 1992; Kurtz, Churchwell, & Wood 1994). Only 4 of the 25 radio sources, VLA 8, VLA 12, VLA 17, and VLA 18, lack a previously reported counterpart.

Of the 25 sources detected, 8 were found to be time variable over the observed timescale of a few days (see column 5 in Table 1). We searched for linear and circular polarization in the sample and only one source (VLA 24) showed left circular polarization at the 3% level. We measured the angular size of the sources using the AIPS task IMFIT, with a correction for bandwidth smearing. With the exception of sources VLA 8, VLA 13, and VLA 19, all sources were found to be unresolved, $\theta_s \leq 0\farcs2$.

We found radio continuum sources closely associated with three of the six submm sources of Mezger et al. (1988), namely FIR 4 (VLA 9), FIR 5 (VLA 10) and FIR 6 (VLA 14). All three sources are relatively weak and do not show time variability. Remarkably, none of these three radio sources have a near-IR or X-ray counterpart, suggesting very large extinction toward them.

Two close ($\leq 2''$) double systems, formed by sources VLA 12 and 13, as well as VLA 15

and 16, respectively, are part of the cluster. Most probably they constitute physical binaries.

4. COMMENTS ON SELECTED INDIVIDUAL SOURCES

4.1. VLA 8

This source has no reported counterparts. It is one of the few sources that is clearly resolved, elongated in the north-south direction (see Fig. 3). Its deconvolved dimensions are $0\farcs59\pm0\farcs03\times0\farcs25\pm0\farcs02; PA = 177^\circ\pm3^\circ$. These angular dimensions correspond to 170 AU $\times$ 95 AU. One possible explanation is that we are observing a thermal radio jet (e. g. Rodríguez 1997) that could be powering the unipolar redshifted CO jet in the region (Richer, Hills, & Padman 1992), since both the radio source and the CO jet are well aligned and elongated in the north-south direction. However, the CO jet seems to emanate from a point about $1'$ south of VLA 8, a position much closer to VLA 10 (=FIR 5). Furthermore, the detailed shape of the source is curved, unlike most thermal jets that are rather straight. This curved morphology is reminiscent of that seen in cometary H II regions or in ionized proplyds. It is known that the ionized Orion proplyds, when observed in the radio continuum (Henney et al. 2002), show an arc-shaped structure. Furthermore, the physical dimensions of VLA 8 are similar to those of the Orion proplyd LV 2 (Henney et al. 2002). Clearly, additional observations are needed to establish if this radio source is a thermal jet, a cometary H II region, or a proplyd. As we will see below, the fact that the arc "points" to the region where the ionizing star of the region is believed to be located favors the identification of this source as a radio proplyd.

4.2. VLA 9

This source has no reported near-IR or X-ray counterpart. It is associated with FIR 4, one of the small-scale submm condensations reported by Mezger et al. (1988), and is thus likely to represent a deeply embedded protostar. It is associated with an infrared reflection nebula (Moore & Yamashita 1995) and a unipolar redshifted CO outflow (Chandler & Carlstrom 1996).

4.3. VLA 10

This source has no reported near-IR or X-ray counterpart, but it is associated with FIR 5 (Mezger et al. 1988). It could be the powering source of the unipolar redshifted CO jet studied by Richer et al. (1992) and Chandler & Carlstrom (1996) since it is located at the position from where this jet seems to originate. Wiesemeyer et al. (1997) present interferometric 3 mm continuum observations, and show that FIR 5 separates into two clumps, FIR 5e and 5w. VLA 10 coincides precisely with FIR 5w. Lai et al. (2002) studied the detailed magnetic field structure around FIR 5.

4.4. VLA 12 and VLA 13

These two sources (see Fig. 4) form a close binary system separated by $0\farcs9$, which at 415 pc corresponds to 375 AU in projection. Source 12 has no reported counterpart. The source VLA 13 is angularly resolved, with deconvolved dimensions of $0\farcs46\pm0\farcs03\times0\farcs12\pm0\farcs04$; $PA = 110^\circ \pm 3^\circ$. Its arc-shaped morphology and the fact that it points to the region where the ionizing star of the region is believed to be located favors, as in the case of VLA 8, the identification of VLA 13 as a radio proplyd.

4.5. VLA 14

This source has no reported near-IR or X-ray counterpart. It is associated with FIR 6 (Mezger et al. 1988) and could be the powering source of a compact bipolar CO outflow found in this region (Richer 1990; Chandler & Carlstrom 1996) since the outflow emanates from a position coincident with VLA 14.

4.6. VLA 15 and VLA 16

Both these VLA objects are 2MASS and Chandra sources. They form a close binary system (see Fig. 5) separated by $1\farcs7$. The source VLA 15 coincides positionally with the infrared source IRS2b, that has been proposed to be the ionizing source of the NGC 2024 H II region by Bik et al. (2003). The source IRS2b, first found by Jiang et al. (1984) and Nisini et al. (1994), is located about $5''$ north-west of IRS2. IRS2 is the brightest near-IR source of this region (detected by us as VLA 19, see below). The source VLA 16 is not detected in the near-IR, but it is a Chandra source (Skinner et al. 2003).

4.7. VLA 17

This source has no reported counterparts. It is located exactly over the sharp ionization front that runs east-west (Barnes et al. 1989). It could be a bright knot in the ionization front, with no young star directly associated.

4.8. VLA 19

This is the brightest radio source in the cluster, with near-IR and X-ray counterparts. It was reported previously as a radio source by Snell & Bally (1986), Gaume et al. (1992), and Kurtz et al. (1994). We found no significant variability at the three epochs observed by us. However, our 3.6 cm flux density of 17.4 mJy is about twice the value of 8.9 mJy reported by Kurtz et al. (1994), from VLA observations taken 13 years before. This radio source coincides with the infrared source IRS2 (Grasdalen 1974; Barnes et al. 1989). The radio source (Fig. 6) clearly shows structure. There is a bright, dominant component to the west, with a fainter extension to the east. At present it is not possible to establish if we are observing a binary source, an ultracompact H II region, or a radio proplyd. Multifrequency observations at high angular resolution are needed to favor one of these possibilities.

4.9. VLA 21

This source is quite bright in the radio and exhibits large variation with a factor of 5.7. It has a Chandra counterpart.

4.10. VLA 24

This source, with 2MASS and Chandra counterparts, is the only one that showed evidence of polarization, showing left circular polarization at the 3% level at all three epochs observed. It is also time variable with variations of about a factor of 2. The combination of fast time variability with circular polarization is an indicator of gyrosynchrotron emission (Feigelson & Montmerle 1999).

5. DISCUSSION

There are several mechanisms that can produce compact centimeter radio sources in regions of star formation. In regions of low mass star formation, thermal jets and gyrosynchrotron emitters can be present. In regions of high mass star formation we also have strong ionizing radiation available and, in addition to the two mechanisms present in low mass star-forming regions, we can have ionized stellar winds, ultracompact H II regions, and radio proplyds. It is possible to distinguish between these various possibilities with high angular resolution, multifrequency observations made with the required sensitivity. For NGC 2024 we only have available the 3.6 cm observations presented here. We can, however, argue that because of its time variability and circular polarization, VLA 24 is most probably a young low mass star showing gyrosynchrotron emission. In the case of sources VLA 2, 5, 6, 11, 20, 21, and 23, their fast time variability suggests also a gyrosynchrotron nature.

Sources VLA 8 and VLA 13 are probably radio proplyds given their morphology and orientation. If so, they can be used in an attempt to search for the ionizing source of the region. These two sources are also affected by bandwidth smearing, but the deconvolution made correcting for this effect clearly shows that they are truly extended. In Figure 7 we show an image that includes these two sources as well as other nearby sources. In this image we have passed two lines by each of the sources. These lines have position angles of ± 3 σ with respect to the perpendicular to the major axes of the sources. The set of lines defines a four-sided region that includes VLA 15 (= IRS2b) and VLA 19 (=IRS2), as can be seen in Fig. 7. Given the uncertainties of the method, we cannot favor either of the sources conclusively. We note, however, that the morphology of VLA 19 (=IRS2) is suggestive also of a proplyd nature (see discussion in section 4.8 as well as Fig. 6). If this is the case, then the object VLA 15 (= IRS2b) is clearly favored as the ionizing source of the region, in agreement with Bik et al. (2003).

Over the years, a few examples of radio clusters associated with regions of recent star formation have been appearing in the literature (Garay et al. 1987; Churchwell et al. 1987; Becker & White 1988; Stine & O'Neal 1998; Rodríguez et al. 1999; Gómez et al. 2000; Lang et al. 2001). In Table 2 we summarize the parameters of these radio clusters. Although more such clusters should be studied to have a reliable statistical base, some interesting trends are evident. The diameters of the radio clusters are in the 0.2 to 0.7 pc range. The radio luminosity of the most luminous member is correlated with the bolometric luminosity of the cluster. We believe that sensitive, high angular resolution studies similar to that presented here are needed to establish if these clusters are always present in other relatively nearby regions of massive star formation. If properly understood, these radio clusters could be an invaluable observational tool to study the stellar population of heavily obscured regions of

star formation.

6. CONCLUSIONS

We have presented sensitive, high angular resolution (0.″2) VLA observations at 3.6 cm toward the NGC 2024 region of recent star formation. Our main conclusions are summarized below.

1. We detected a total of 25 compact radio sources in a region of $4' \times 4'$. Only four of these sources do not have a previously reported counterpart at any wavelength. However, only one of the radio sources had been reported in the literature.

2. We found radio continuum sources closely associated with three of the six submm sources in the region. Remarkably, none of these three radio/submm sources has a near-IR or X-ray counterpart, suggesting very large extinction toward them.

3. Two of the sources (VLA 8 and VLA 13) are proposed to be radio proplyds whose study may help pinpoint the origin of the ionizing radiation in the region. Our attempts to do this suggest a region containing both VLA 15 (= IRS2b) and VLA 19 (=IRS2) as the area where the ionizing source is located.

4. The source VLA 19, the counterpart of IRS2, is found to exhibit spatial structure, although its precise nature remains undetermined. We also detected a radio counterpart to IRS2b, the source that has been recently proposed to be ionizing NGC 2024.

5. Eight of the sources detected (VLA 2, 5, 6, 11, 20, 21, 23, and 24) show fast time variability and probably are young low mass stars exhibiting gyrosynchrotron emission.

6. Two close ($\leq 2''$) binary systems, formed by sources VLA 12 and 13 and VLA 15 and 16, respectively, are part of the cluster.

7. We have briefly discussed the parameters of other radio clusters found in regions of star formation and suggest that sensitive, high angular resolution studies of other relatively nearby massive star formation regions are likely to detect similar clusters.

We thank Will Henney for his comments on proplyds and Steve Skinner for providing us with his list of X-ray sources before publication. We are also grateful to George Herbig for calling our attention to the radio cluster in NGC 1579. LFR and YG acknowledge the support of DGAPA, UNAM, and of CONACyT (México). BR acknowledges support from

NASA grant NAG5-8108. The Second Palomar Observatory Sky Survey (POSS-II) was made by the California Institute of Technology with funds from the National Science Foundation, the National Aeronautics and Space Administration, the National Geographic Society, the Sloan Foundation, the Samuel Oschin Foundation, and the Eastman Kodak Corporation. The Oschin Schmidt Telescope is operated by the California Institute of Technology and Palomar Observatory. The 2MASS project is a collaboration between The University of Massachusetts and the Infrared Processing and Analysis Center (JPL/ Caltech), with funding provided primarily by NASA and the NSF. This research has made use of the SIMBAD database, operated at CDS, Strasbourg, France.

REFERENCES

Anthony-Twarog, B. J. 1982, AJ, 87, 1213

Barnes, Peter J., Crutcher, R. M., Bieging, J. H., Storey, J. W. V., & Willner, S. P. 1989, ApJ, 342, 883

Beck, T. L., Simon, M., & Close, L. M. 2003, ApJ, 583, 358

Becker, R. H. & White, R. L. 1988, ApJ, 324, 893

Bik, A., Lenorzer, A., Kaper, L., Comerón, F., Waters, L. B. F. M., de Koter, A., & Hanson, M. M. 2003, A&A, 404, 249

Chandler, C.J., & Carlstrom, J.E. 1996, ApJ, 466, 338

Churchwell, E., Wood, D. O. S., Felli, M., & Massi, M. 1987, ApJ, 321, 516

Feigelson, E. D. & Montmerle, T. 1999, ARAA, 37, 363

Fomalont, E. B., Kellermann, K. I., Partridge, R. B., Windhorst, R. A., & Richards, E. A. 2002, AJ, 123, 2402

Garay, G., Moran, J. M., & Reid, M. J. 1987, ApJ, 314, 535

Gaume, R. A., Johnston, K. J., & Wilson, T. L. 1992, ApJ, 388, 489

Gómez, Y., Rodríguez, L. F., & Garay, G. 2000, ApJ, 531, 861

Gómez, Y., Rodríguez, L. F., & Garay, G. 2002, ApJ, 571, 901

Grasdalen, G.L. 1974, ApJ, 193, 373

Haisch, K. E., Lada, E. A., & Lada, C. J. 2000, AJ, 120, 1396

Haisch, K. E., Lada, E. A., Piña, R. K., Telesco, C. M., & Lada, C. J. 2001, AJ, 121, 1512

Henney, W. J., O'Dell, C. R., Meaburn, J., Garrington, S. T., & Lopez, J. A. 2002, ApJ, 566, 315

Jiang, D.R., Perrier, C., & Léna, P. 1984, A&A, 135, 249

Kurtz, S., Churchwell, E., & Wood, D. O. S. 1994, ApJS, 91, 659

Lada, E. A.; Evans, N. J., Depoy, D. L., & Gatley, I. 1991, ApJ, 371, 171

Lai, S.-P., Crutcher, R. M., Girart, J. M., & Rao, R. 2002, ApJ, 566, 925

Lang, C. C., Goss, W. M., & Rodríguez, L. F. 2001, ApJ, 551, L143

Menten, K. M. & Reid, M. J. 1995, ApJ, 445, L157

Mezger, P. G., Chini, R., Kreysa, E., Wink, J. E., & Salter, C. J. 1988, A&A, 191, 44

Moore, T. J. T., & Chandler, C. J. 1989, MNRAS, 241, 19

Moore, T.J.T., & Yamashita, T. 1995, ApJ, 440, 722

Nisini, B., Smith, H.A., Fischer, J., & Geballe, T.R. 1994, A&A, 290, 463

Richer, J. S., Hills, R. E., & Padman, R. 1992, MNRAS, 254, 525

Richer, J. S. 1990, MNRAS, 245, 24

Rodríguez, L. F. & Chaisson, E. J. 1978, ApJ, 221, 816

Rodríguez, L.F. 1997, in IAU Symp. No. 182 *Herbig-Haro Flows and the Birth of Low Mass Stars*, Eds. B. Reipurth & C. Bertout, Kluwer, p. 83

Rodríguez, L.F., Anglada, G., & Curiel, S. 1999, ApJS, 125, 427

Schulz, A., Guesten, R., Zylka, R., & Serabyn, E. 1991, A&A, 246, 570

Skinner, S., Belzer, E., & Gagne, M. 2003, ApJ, submitted.

Snell, R. L. & Bally, J. 1986, ApJ, 303, 683

Stine, P. C. & O'Neal, D. 1998, AJ, 116, 890

Visser, A.E., Richer, J.S., Chandler, C.J., & Padman, R. 1998, MNRAS, 301, 585

Wiesemeyer, H., Güsten, R., Wink, J.E., & Yorke, H.W. 1997, A&A, 320, 287

Fig. 1.— VLA continuum image of NGC 2024 at 3.6 cm. The contour shown is 6 times 15 μJy beam^{-1}, the rms noise of the image. The half power full width of the circular restoring beam is $0\farcs24$. The compact sources are numbered from VLA 1 to VLA 25. The faint emission features that appear to the east and west of source VLA 17 are part of the ionization front and are not considered individual compact sources.

Fig. 2.— Position of the compact radio sources detected, overlapped on a greyscale image of the region from the red Digital Sky Survey. The position and number of some of the sources are shown in white so that are seen better against the dark background.

Fig. 3.— VLA continuum image of NGC 2024 VLA 8 at 3.6 cm. The contours are -4, 4, 5, 6, 8, 10, 12, 15, and 20 times 15 μJy beam^{-1}, the rms noise of the image. The half power contour of the circular restoring beam is shown in the bottom left corner.

Fig. 4.— VLA continuum image of the sources NGC 2024 VLA 12 and 13 at 3.6 cm. The contours are -4, 4, 5, 6, 8, 10, and 12 times 15 μJy beam^{-1}, the rms noise of the image. The half power contour of the circular restoring beam is shown in the bottom left corner.

Fig. 5.— VLA continuum image of the sources NGC 2024 VLA 15 and 16 at 3.6 cm. The contours are -4, 4, 5, 6, 8, 10, 12, 15, 20, and 30 times 15 μJy beam^{-1}, the rms noise of the image. The half power contour of the circular restoring beam is shown in the bottom left corner. The north-south elongation of the sources is due to the bandwidth smearing aberration.

Fig. 6.— VLA continuum image of the source NGC 2024 VLA 19 at 3.6 cm. The contours are -5, 5, 6, 8, 10, 12, 15, 20, 30, 40, 60, 80, 100, 150, 200, 300, and 400 times 15 μJy beam^{-1}, the rms noise of the image. The half power contour of the circular restoring beam is shown in the bottom left corner. The north-south elongation of the source is due to the bandwidth smearing aberration.

Fig. 7.— VLA continuum image of several sources in the core of NGC 2024 at 3.6 cm. The contour shown is 6 times 15 μJy beam^{-1}, the rms noise of the image. The dashed lines have position angles of ±3 σ with respect to the perpendicular to the major axes of the sources VLA 8 and VLA 13. These lines define a four-sided region that includes sources VLA 15 (IRS2b) and VLA 19 (IRS2). Note that the ten VLA sources in this Figure are distributed in the plane of the sky approximately in an ellipse.

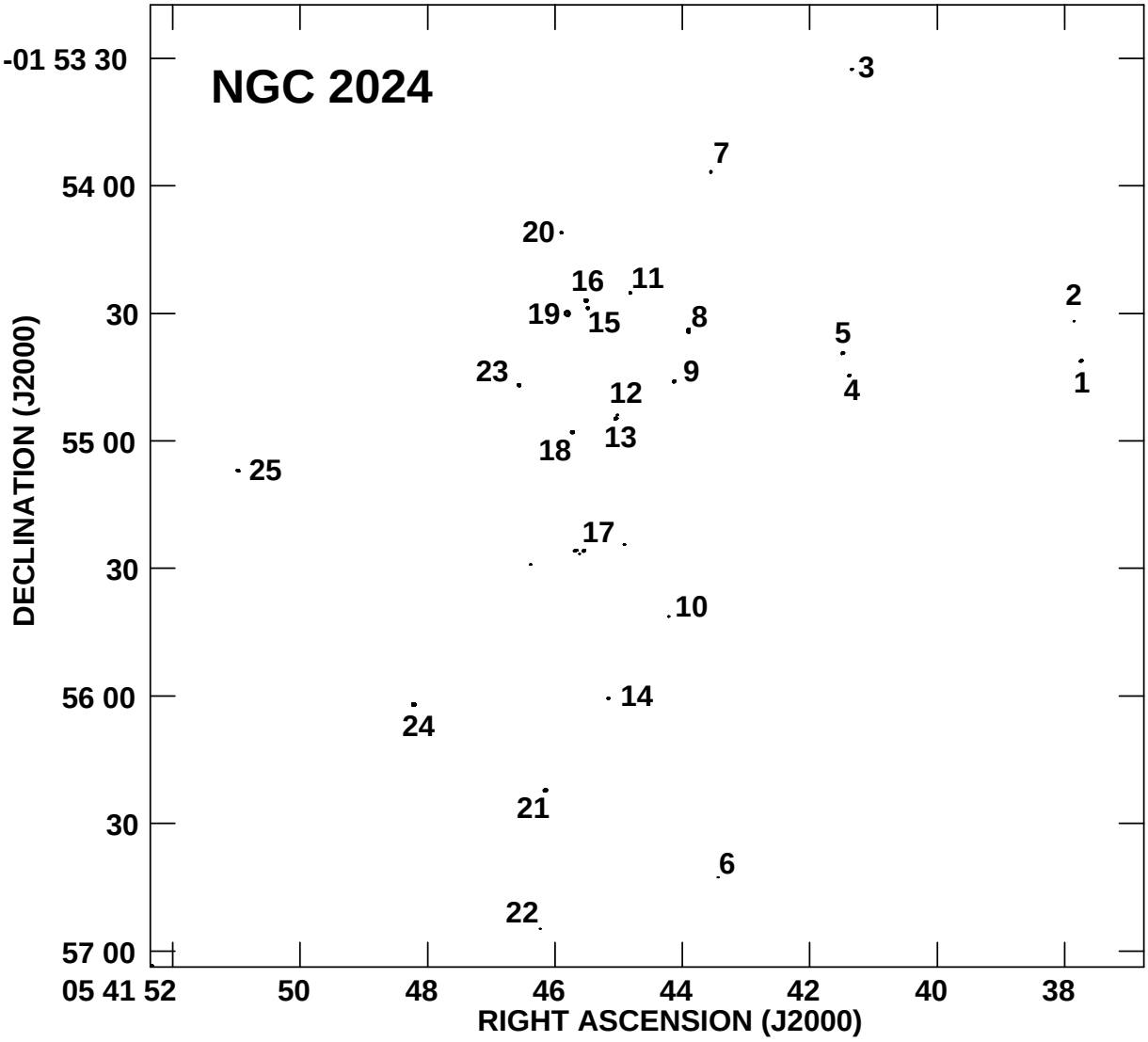
NGC 2024
-01 53 30
54 00
30
55 00
30
56 00
30
57 00
DECLINATION (J2000)
05 41 52
50
48
46
44
42
40
38
RIGHT ASCENSION (J2000)
1
2
3
4
5
6
7
8
9
10
11
12
13
14
15
16
17
18
19
20
21
22
23
24
25

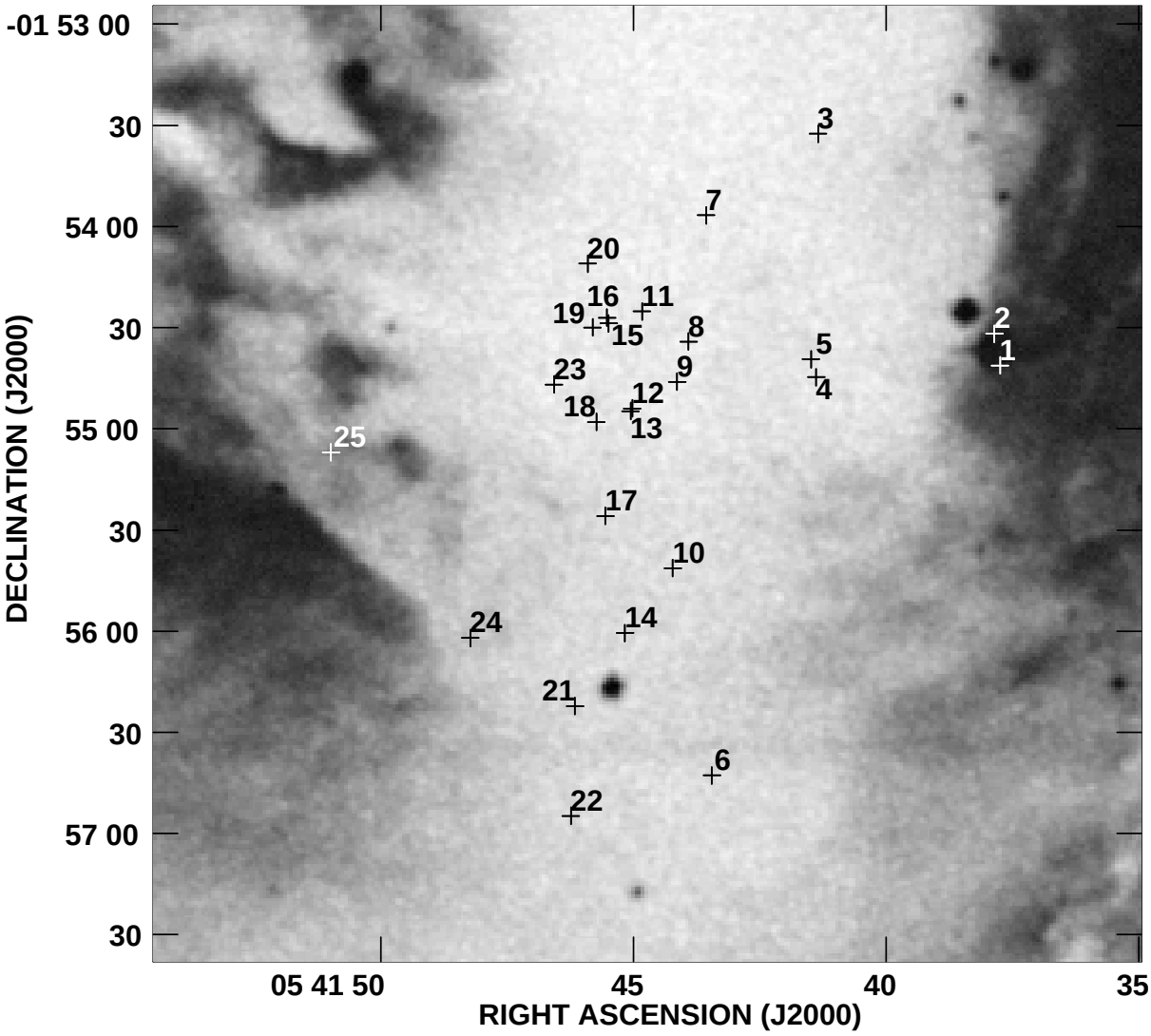
-01 53 00
30
54 00
30
55 00
30
56 00
30
57 00
30
DECLINATION (J2000)
05 41 50
45
40
35
RIGHT ASCENSION (J2000)
1
2
3
4
5
6
7
8
9
10
11
12
13
14
15
16
17
18
19
20
21
22
23
24
25

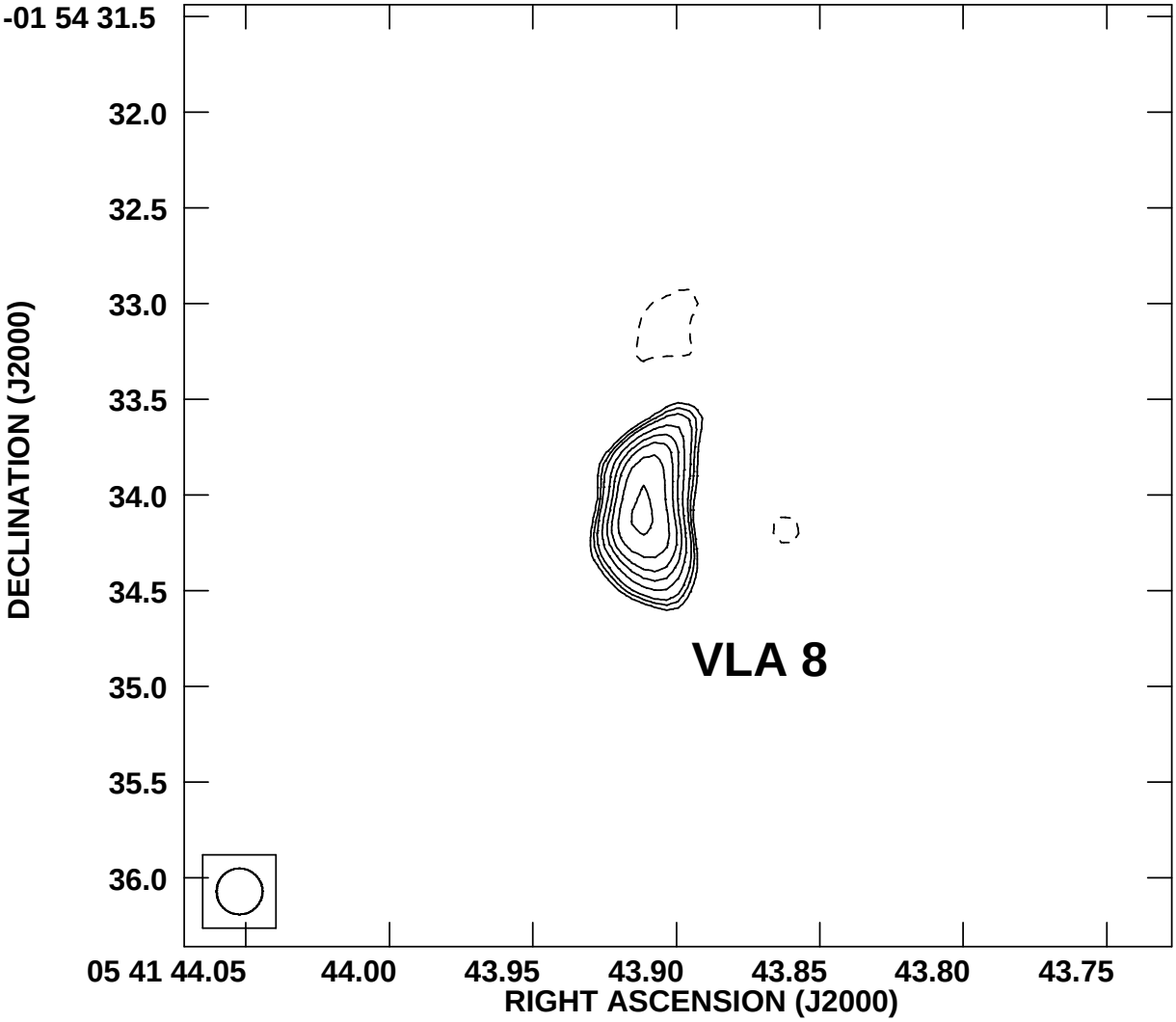
-01 54 31.5
32.0
32.5
33.0
33.5
34.0
34.5
35.0
35.5
36.0
DECLINATION (J2000)
VLA 8
05 41 44.05
44.00
43.95
43.90
43.85
43.80
43.75
RIGHT ASCENSION (J2000)

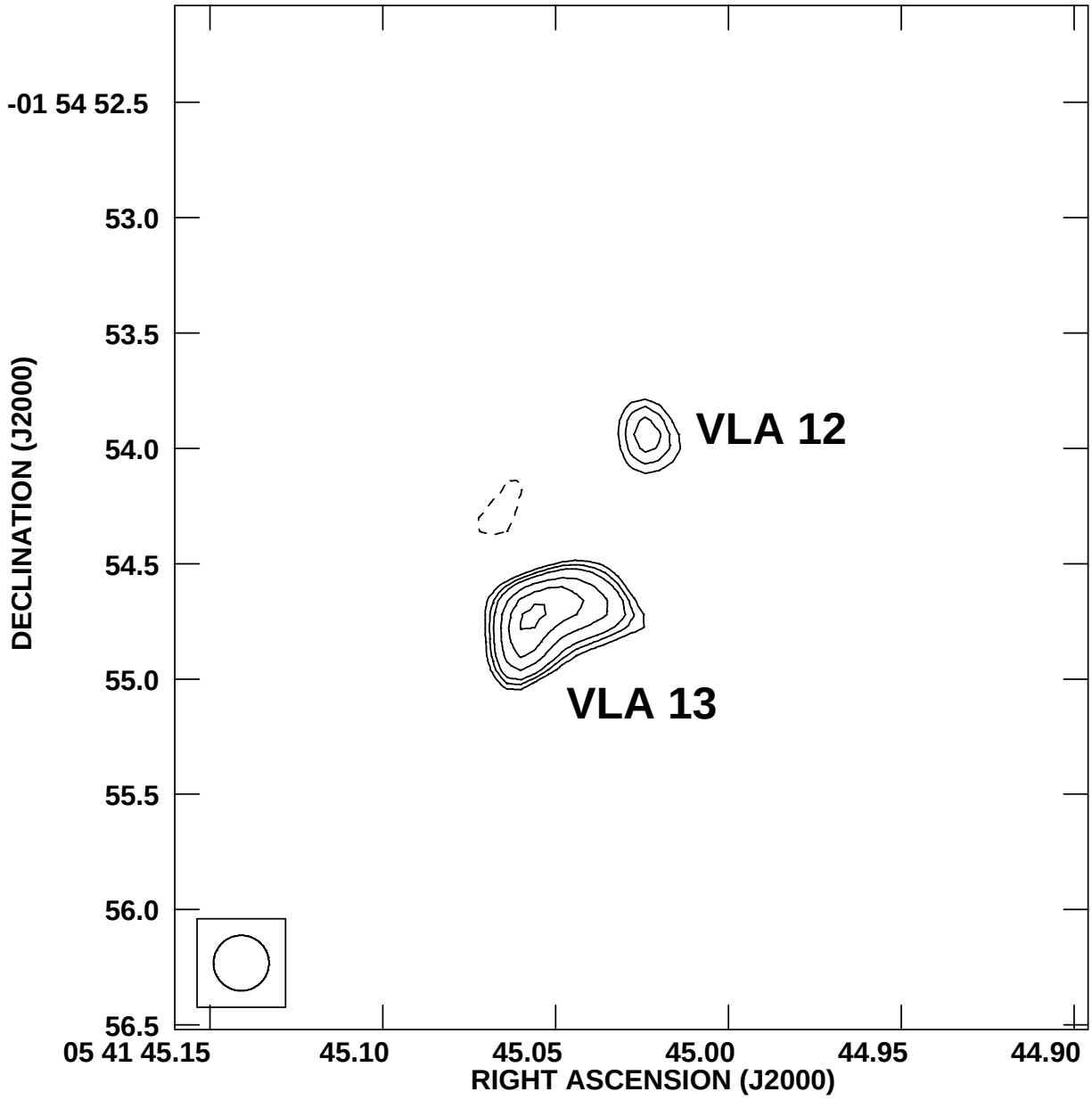
-01 54 52.5
53.0
53.5
54.0
54.5
55.0
55.5
56.0
56.5
DECLINATION (J2000)
VLA 12
VLA 13
05 41 45.15
45.10
45.05
45.00
44.95
44.90
RIGHT ASCENSION (J2000)

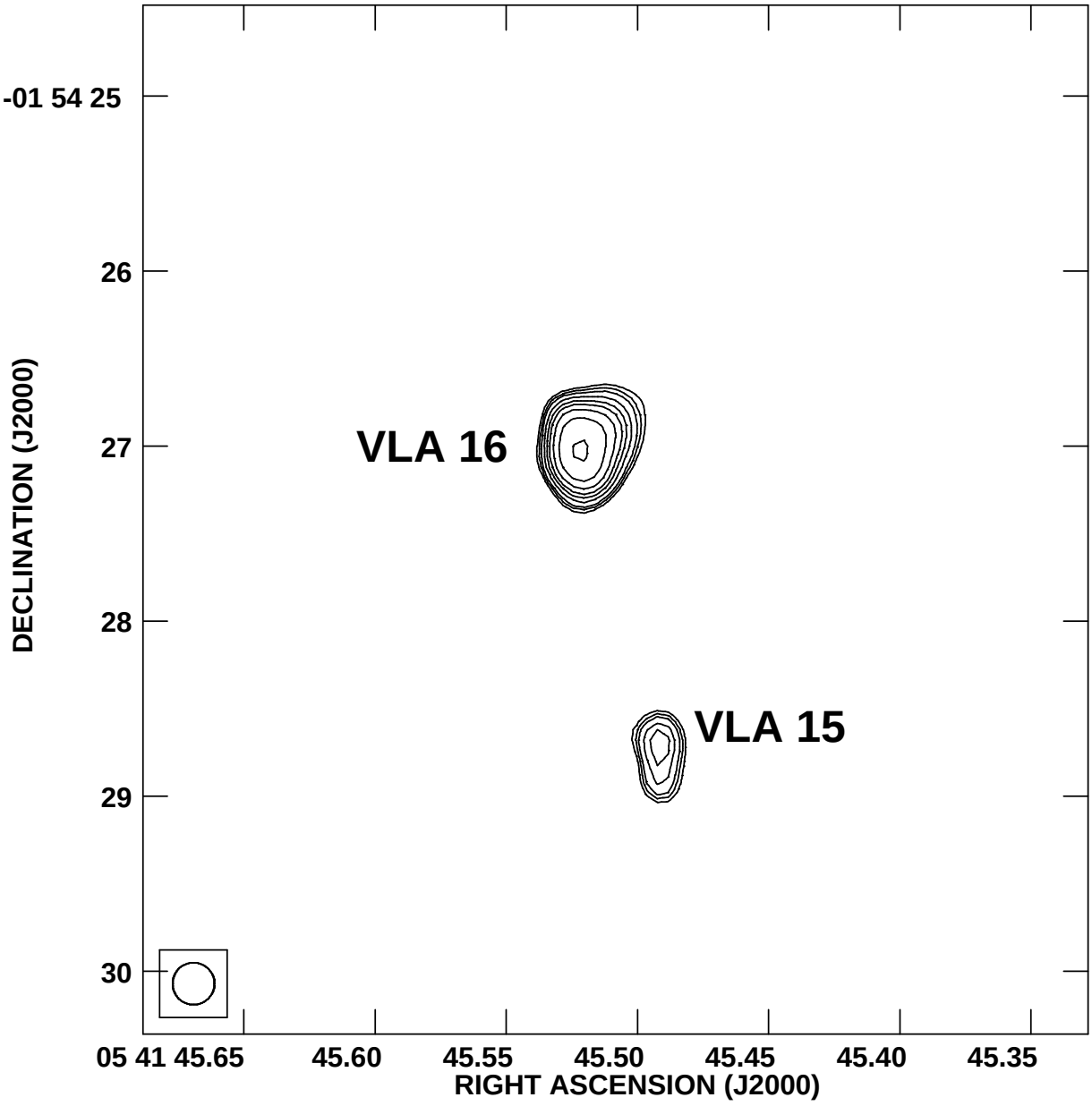
-01 54 25
26
27
28
29
30
DECLINATION (J2000)
VLA 16
VLA 15
05 41 45.65
45.60
45.55
45.50
45.45
45.40
45.35
RIGHT ASCENSION (J2000)

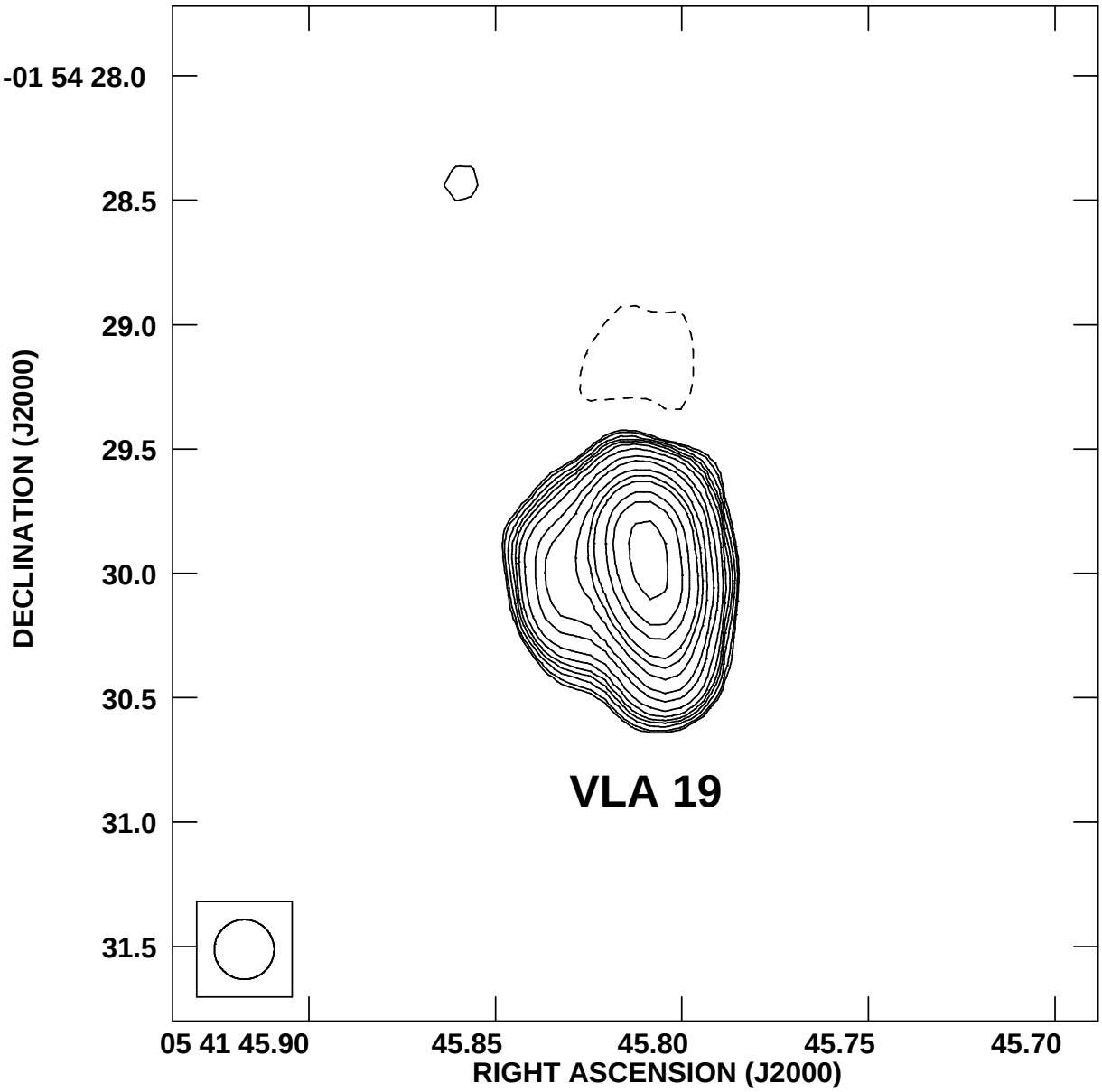
-01 54 28.0
28.5
29.0
29.5
30.0
30.5
31.0
31.5
DECLINATION (J2000)
VLA 19
05 41 45.90
45.85
45.80
45.75
45.70
RIGHT ASCENSION (J2000)

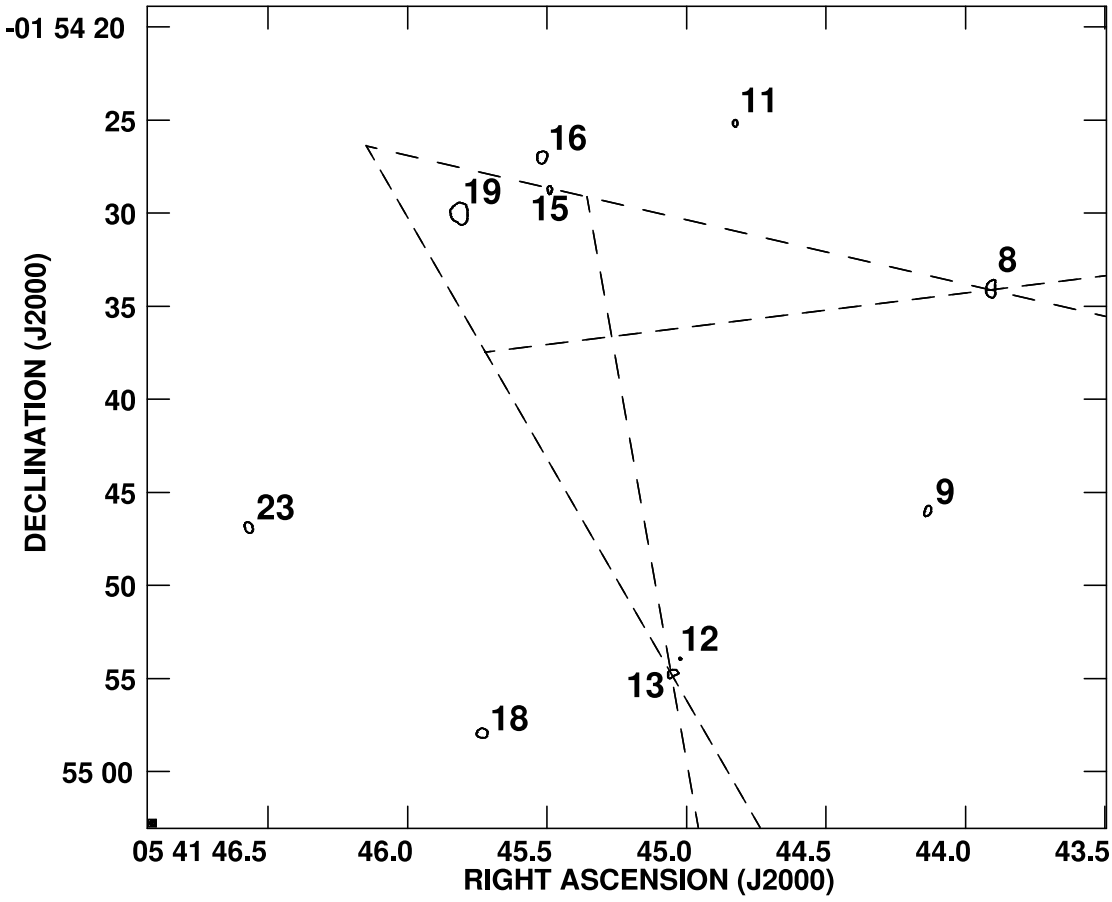
-01 54 20
25
30
35
40
45
50
55
55 00
DECLINATION (J2000)
05 41 46.5
46.0
45.5
45.0
44.5
44.0
43.5
RIGHT ASCENSION (J2000)
11
16
19
15
8
23
9
12
13
18

Table 1. Parameters of the 3.6 cm VLA Sources

VLA	R.A. α_{2000}	Dec. δ_{2000}	Flux[a] (mJy)	Time Variable?	Counterpart[b] 2MASS	Chandra	Other
1	05 41 37.745	-01 54 41.20	0.30	N			HLP 2
2	05 41 37.858	-01 54 31.82	0.16	Y(1.9)	05413786-0154323	SGB 78	
3	05 41 41.346	-01 53 32.54	0.28	N	05414134-0153326	SGB 120	HLL 52, BSC 69
4	05 41 41.385	-01 54 44.64	0.26	N	05414138-0154445	SGB 123	
5	05 41 41.487	-01 54 39.35	0.33	Y(3.7)	05414148-0154390	SGB 124	HLL 87, BSC 65
6	05 41 43.446	-01 56 42.74	0.10	Y(6.5)	05414344-0156425	SGB 147	BCB IRS24
7	05 41 43.559	-01 53 56.67	0.20	N	05414356-0153567	SGB 152	
8	05 41 43.912	-01 54 34.13	0.63	N			
9	05 41 44.136	-01 54 46.04	0.33	N			M FIR 4, MC89-4
10	05 41 44.221	-01 55 41.32	0.11	N			M FIR 5, LCGR FIR 5 4
11	05 41 44.827	-01 54 25.16	0.22	Y(1.6)	05414482-0154251	SGB 171	HLL 77, HLP 22
12	05 41 45.024	-01 54 53.94	0.11	N			
13	05 41 45.056	-01 54 54.73	0.24	N	05414504-0154546		
14	05 41 45.168	-01 56 00.56	0.29	N			M FIR 6, LCGR FIR 6 n
15	05 41 45.492	-01 54 28.70	0.24	N	05414550-0154286	SGB 182	B IRS2b
16	05 41 45.522	-01 54 27.02	0.97	N		SGB 183	
17	05 41 45.554	-01 55 25.86	0.27	N			
18	05 41 45.733	-01 54 57.93	0.49	N			
19	05 41 45.809	-01 54 29.92	17.4	N	05414580-0154297	SGB 187	IRS2, KCW 206.543-16.347
20	05 41 45.905	-01 54 10.98	0.18	Y(5.0)		SGB 188	BSC 93
21	05 41 46.157	-01 56 22.20	4.54	Y(5.7)		SGB 193	
22	05 41 46.236	-01 56 54.80	0.10	N		SGB 196	
23	05 41 46.570	-01 54 46.88	1.17	Y(6.2)	05414655-0154469	SGB 200	
24	05 41 48.224	-01 56 02.01	8.60	Y(2.2)	05414821-0156020	SGB 210	
25	05 41 50.983	-01 55 06.97	0.24	N	05415096-0155070		HLP 29, HLL 98

Note. — (a): Total flux density corrected for primary beam response. The flux density reported is the average of the three epochs observed.
(b): B = Bik et al. 2003; BCB = Barnes et al. 1989; BSC = Beck et al. 2003; HLL = Haisch et al. 2000; HLP = Haisch et al. 2001; KCW = Kurtz et al. 1994; LCGR = Lai et al. 2002; M = Mezger et al. 1988; MC = Moore & Chandler 1989; SGB = Skinner, Gagné, & Belzer 2003.

Table 2. Parameters of Radio Clusters in Regions of Recent Star Formation

Region	Luminosity ($L_\odot$)	Number of Members	Most Luminous Member (mJy kpc^2)[a]	Diameter (pc)	Reference
Orion	$\sim 2 \times 10^5$	∼50	8.8	0.3	Menten & Reid (1995)
NGC 1579	$\sim 2 \times 10^3$	16	0.6	0.3	Stine & O'Neal (1998)
GGD 14	$\sim 10^4$	6	0.2	0.2	Gómez et al. (2002)
NGC 1333	~ 120	44	0.3	0.7	Rodríguez et al. (1999)
Arches	$\sim 10^7$	8	122.8	0.7	Lang et al. (2001)
NGC 2024	$\sim 5 \times 10^4$	25	3.0	0.5	This paper

Note. — (a): 3.6 cm flux density times distance in kpc squared